CFD simulation of stratified indoor environ ment in displacement ventilation: Validation and sensitivity analysis

S. Gilani[1,*], H. Montazeri[2], B. Blocken[2,3]

[1]*School of Architecture, University of Tehran, P.O. Box 14155-6458, Enghelab Avenue, Tehran, Iran*

[2]*Building Physics and Services, Department of the Built Environment, Eindhoven University of Technology, P.O. Box 513, 5600 MB Eindhoven, The Netherlands*

[3]*Building Physics Section, Department of Civil Engineering, Leuven University, Kasteelpark Arenberg 40 – Bus 2447, 3001 Leuven, Belgium*

Abstract

Knowledge of temperature stratification in indoor environments is important for occupant thermal comfort and indoor air quality and for the design and evaluation of displacement ventilation systems. This paper presents a detailed and systematic evaluation of the performance of 3D steady Reynolds-Averaged Navier-Stokes (RANS) CFD simulations to predict the temperature stratification within a room with a heat source and two ventilation openings. The indoor air quality within the room is also investigated by assessing the distribution of the age of air. The evaluation is based on validation with full-scale measurements of air temperature. A sensitivity analysis is performed to investigate the impact of computational grid resolution, turbulence model, discretization schemes and iterative convergence on the predicted temperatures and age of air. The results show that steady RANS with the SST k-ω model can accurately predict the temperature stratification in this particular indoor environment. However, of the five commonly used turbulence models, only the SST k-ω model and the standard k-ω model succeed in reproducing the thermal plume structure and the associated thermal stratification, while the three k-ε models clearly fail in doing so. In addition, the iterative convergence criteria have a major impact on the predicted age of air, where it is shown that very stringent criteria in terms of scaled residuals are required to obtain accurate results. These required criteria are much more stringent than typical default settings. This paper is intended to contribute to improved accuracy and reliability of CFD simulations for displacement ventilation assessment.

Keywords: Computational Fluid Dynamics (CFD); Displacement ventilation; Buoyancy-driven ventilation; Temperature stratification; Turbulence modeling; Age of air.

1. Introduction

Temperature stratification in indoor environments, generated by heat sources such as heating systems, occupants, electronic equipment and solar radiation on interior surfaces, can affect occupant thermal comfort. In addition, in higher building spaces, such as atria, temperature stratification can be considered as one of the main issues for providing thermal comfort in the lower and upper adjacent spaces. This phenomenon also affects the indoor air quality that can be assessed by the local age of air [1-4], which can exhibit pronounced vertical gradients. Therefore, knowledge of temperature stratification in building spaces is required to improve occupant thermal comfort and indoor air quality. This is especially the case when buoyancy-driven ventilation, called displacement ventilation, is incorporated into the design of a building. This mode of ventilation can efficiently purge excess heat and pollutants from interior spaces (e.g. [5-8]).

Research on temperature stratification in enclosed spaces can be performed by different methods: full-scale measurements [9-15], reduced-scale measurements [16-17], analytical methods [16, 18-21] and Computational Fluid Dynamics (CFD) [11, 14-15, 22]. Building energy simulation is also another method to support designs and development of innovative building system concepts, such as displacement ventilation, under a range of different dynamic operating conditions. However, for performance prediction of stratified indoor environments, this method is generally considered too limited in terms of spatial resolution [23-24]. Full-scale measurements have the advantage of providing the capability to study the real situations in their full complexity. However, in full-scale measurements it is generally not possible to perform measurements in all points in the domain and to control all the boundary conditions (e.g. [23, 25-26]). In reduced-scale laboratory measurements, controlling most boundary conditions is possible, but similarity constraints can be the main concerns [23]. Analytical methods have the advantage of simplicity, potentially providing reliable physical information, without need for powerful computing resources. However, they are generally not reliable for complicated cases concerning both geometry and thermo-fluid boundary conditions [23]. On the other hand, CFD provides detailed flow field data in the whole computational domain and without similarity constraints because simulations can be performed at full scale. It also allows parametric studies to

---

*Corresponding author. Email address: sgilani@ut.ac.ir

be carried out easily and efficiently [14, 23, 25-29]. In addition, the application of CFD for studying indoor air quality (e.g. [30-34]), natural ventilation (e.g. [14-15, 35-40]) and stratified indoor environment (e.g. [41]) is increasing since these are difficult to predict with other methods, as highlighted in some recent review papers [23, 25, 29]. Despite all the mentioned advantages, the accuracy and reliability of CFD simulations remain important concerns and therefore, CFD validation and verification are imperative. This is especially the case for CFD simulation of buoyancy-driven ventilation, in which the flow is normally very complex and depends on many different physical parameters. For this type of ventilation, several CFD validation studies have been performed and the performance of different turbulence models has been evaluated (e.g. [42-55]). However, the conclusions on which turbulence models perform best are not always consistent. For example, the superior performance of the RNG k-ε model has been pointed out in some studies, e.g. [42-43, 45-47, 52, 55], while other studies showed that the SST k-ω model was clearly superior [22, 54, 56-59]. This inconsistency can be related to physical characteristics of the case studies, but also different computational parameters and settings used in different studies. Therefore, there is a strong need for detailed and systematic sensitivity analyses, from which more detailed best practice guidelines can be derived.

For these reasons, this paper presents a detailed evaluation of 3D steady Reynolds-Averaged Navier-Stokes (RANS) CFD simulations to predict the temperature, velocity and air quality in a room with a heat source and two ventilation openings. The evaluation is based on validation with full-scale measurements of air temperature by Li et al. [19, 60]. The impact of the computational grid resolution, turbulence model, discretization schemes and iterative convergence on the CFD results of air temperature, velocity and air quality is investigated. The concept of age of air introduced by Sandberg [61] is used to assess the indoor air quality.

In section 2, the full-scale measurements of indoor air temperature by Li et al. [19, 60] are described. Section 3 explains the computational settings and parameters for the reference case and compares the results of the CFD simulations with those of the experiment. In section 4, the sensitivity analysis is performed. The limitations of the study are discussed in section 5 and the main conclusions are outlined in section 6.

2. Description of full-scale experiment

Full-scale measurements of air temperature for a typical room subjected to displacement ventilation were performed by Li et al. [19, 60]. The test room had inside dimensions width × length × height = 3.6 × 4.2 × 2.75 m^3 (Figure 1). Two sets of experiments were performed to investigate the impact of radiative heat transfer on the air temperature in the room. In the first set, the interior surfaces of the test-room walls were painted black, while in the other one, they were covered with aluminum sheets. The overall heat transmittance values (U-values) of the floor, ceiling and vertical walls1, 2 and 3 (Figure 1) were all equal to 0.36 W/m^{2}K. For wall 4, the U-value was 0.15 W/m^{2}K. Air was supplied into the test room through an inlet at floor level with dimensions width × height = 0.45 × 0.5 m^2, 50 % of which was perforated, resulting in an effective opening area of 0.1125 m^2. The air was extracted from the test room through an outlet with dimensions of width × height = 0.525 × 0.220 m^2 that was located at a height of 2.39 m in wall 2. A prismatic porous heat source with dimensions width × length × height = 0.3 × 0.4 × 0.3 m^3 induced displacement ventilation in the test room. It was placed 0.1 m above the floor level and 2.7 m from the inlet (Figure 1). It incorporated 24 light bulbs of 25 W in total, which were controlled individually to provide different levels of heat load up to 600 W. The main frame of the prism was aluminum and it was filled with aluminum chips to distribute the heat evenly and to avoid short-wave radiation to the wall surfaces.

The air temperature was measured by 30 thermocouples located along a single vertical pole inside the test room (Figure 1). The thermocouples were distributed along the vertical pole with a higher concentration near the floor and ceiling. The interior surface temperatures were measured by 22 thermocouples, five on each wall, one on the ceiling and one on the floor. Two thermocouples measured the inlet and outlet air temperatures. Five thermocouples also measured the exterior surface temperature of the walls and the ceiling. The measurement uncertainty was estimated to be ±0.1°C.

In this experiment, the impacts of different parameters such as heat load, wall emissivity, inlet flow rate and inlet air temperature were investigated through different cases including B1 to B5 and A1 to A4, in which 'B' and 'A' stand for black-painted and aluminum-covered cases, respectively. The experimental data for cases B1, B2, B3 and A2 were reported more completely than the other cases in Refs. [19, 60]. The focus of this paper is on case B1 for which the largest amount of experimental data was provided. In addition, this case had the lowest air change rate (n), which was 1 h^{-1}. Therefore, the air was supplied with a lower velocity and as a result, the flow was not a jet-type flow, which is important in this paper to investigate the stratified properties of air in the room. For this case, the inlet (T_i) and outlet air temperatures (T_o) were 16.0°C and 27.3°C, respectively. The heat load (E) was 300 W.

3. CFD simulations: reference case

In this section, the computational parameters of the reference case are described. These parameters are modified systematically for the sensitivity analysis in the next section.

3.1. Computational grid

A computational model was made for the room used in the full-scale measurement. The computational grid had 451,248 hexahedral cells generated using the surface-grid extrusion method presented by van Hooff and Blocken [14] (Figure 2). The maximum stretching ratio was 1.2. A total number of 6 and 25 cells were used along the length and height of the inlet, respectively. There were 8 and 7 cells for the outlet. The distance from the center point of the wall-adjacent cell to the wall for different surfaces of the room was 0.0005 m. This corresponds to a maximum y^* value of 1.8. As low-Reynolds number modelling was used in this study, this value ensured that a few cells were placed inside the viscous sub-layer.

3.2. Boundary conditions

Two separate zones were specified in the test room: a fluid-type zone for the room air and a solid–type zone for the heat source. Note that in the experiments, the heat source was a porous design. In our simulations, however, the heat source was modelled as a solid body with a constant heat generation rate. A source term was defined for the zone of the heat source with a constant volumetric heat generation (q) of about 8333 W/m^3 according to Eq. (1):

$$q = \frac{E}{V_{hs}}$$

(1)

where E is the heat load (W) and V_{hs} the heat-source volume (m^3).

The incompressible ideal gas law was used to estimate the air density as a function of T [62]. Other properties of the air were determined at the average value of the measured air temperatures along the vertical pole inside the test room (i.e. 24.5°C). In this case, the molecular Prandtl number (Pr) of air was 0.71. The operating pressure and operating density were 101,325 Pa and 1.17 kg/m^3, respectively [63]. For the outlet, zero static pressure was specified. The Rayleigh number (Ra) was calculated to be about 4×10^{10} and therefore, Ra/Pr was 5.6×10^{10} which is in the threshold for the occurrence of turbulent natural convection [62]. The computed Ra corresponds to the following values: density 1.17 kg/m^3, specific heat capacity 1006.95 J/kgK, thermal expansion coefficient 0.003 K^{-1}, characteristic length 2.75 m, temperature difference between average room air and heat source ~200 K, dynamic viscosity 1.83×10^{-5} kg/ms and thermal conductivity 0.026 (W/mK).

The inlet boundary condition was a uniform velocity ($\bar{u}$) (m/s), calculated based on the experimental data using Eq. (2):

$$\bar{u} = \frac{Q}{A_i} = \frac{nV}{A_i}$$

(2)

where Q is the inlet flow rate (m^3/s), A_i the inlet opening area (m^2), n the number of test-room air changes (s^{-1}) and V the test-room volume (m^3). The inlet air temperature (T_i) was 16.0°C according to the experimental data.

A fixed temperature condition was applied for the test-room surfaces. Note that in Ref. [60] the interior surface temperature of the vertical walls was provided as the average value of the measured temperatures of the walls at five different heights (Table 1). In the CFD simulations, the same values were used to define the surface temperature of the walls assuming that the temperature in between these heights varied linearly with height (Figure 3).

Although the interior surface temperature of the floor and the ceiling were measured in the experiment, their values were not mentioned in Ref. [60]. Therefore, in the present paper, the interior surface temperatures of the floor and the ceiling had to be estimated using the procedure outlined below, although it should be acknowledged that this procedure entails quite some assumptions. It is expected that deviations between these estimates and the actual values will change the absolute values of temperature and age of air in the room, but not the observed trends of the validation and sensitivity analysis. Two reasons can support this expectation. First, the comparison – albeit limited - of the numerically simulated temperatures with the measured values shows quite a good agreement along the vertical pole, including the regions near the floor and ceiling (will be explained in Sec. 3.4). Second, the trends, e.g. concerning turbulence model performance (see Figure 10) are very pronounced, most likely beyond the limited influence of potentially small deviations in the floor and ceiling temperatures.

The floor surface temperature was calculated using Eq. (3) [19]. This equation is for a room ventilated by displacement ventilation, and three zones were assumed in the room: the zone just above the floor, the zone just below the ceiling and the region in-between. The temperature profile was assumed to vary linearly with height in each zone. In addition, the supplied air and exhausted air were assumed to spread evenly in the region just above the floor and just below the ceiling, respectively. Eq. (3) expresses the heat balance in the zone just above the floor and represents that the supplied air is heated by convection near the floor surface. Note that this is an approximation needed because of the lack of experimental data in [60]. This equation was developed and used by Li et al. [19].

$$T_{if} = \frac{\rho \, c_p \, Q \, (T_f^a - T_i)}{h_{ci} A_f} + T_f^a$$

(3)

3

where T_{if} is the floor surface temperature, ρ the air density (kg/m³), c_p the specific heat capacity of air (J/kgK), Q the inlet flow rate (m³/s), T_f^a the near-floor air temperature (the nearest measured air temperature to the floor, i.e. 22.8°C) and T_i the inlet air temperature (16.0°C). h_{ci} is the interior convective heat transfer coefficient (5 W/m²K) according to ISO 6946 [64] and A_f the floor surface area (m²). In this case, the interior surface temperature of the floor (T_{if}) obtained by Eq. (3) was 24.0°C.

The interior surface temperature of the ceiling (T_{ic}) was calculated by applying the energy conservation equation for the ceiling-room interface as shown in Figure 4. There are three heat transfer mechanisms for this control surface: conduction from the ceiling to the control surface (q''_{cond}), convection from the ceiling to the air inside the room (q''_{conv}) and radiation from the ceiling to the surroundings (q''_{rad}) as shown in Eqs. (4) and (5):

$$q''_{cond} = q''_{conv} + q''_{rad} \tag{4}$$

$$\frac{k}{L}(T_{ec} - T_{ic}) = h_i(T_{ic} - T_\infty) + \sum_{j=1}^{j=25} \sigma \varepsilon_{ic} F_{ic \to j}(T_{ic}^4 - T_{surf(j)}^4) \tag{5}$$

where k is the thermal conductivity of the ceiling material (W/mK), L the ceiling thickness (m), T_{ec} the exterior surface temperature of the ceiling (K) (20.3°C = 293.45 K), T_{ic} the interior surface temperature of the ceiling (K) and h_i the interior convective heat transfer coefficient (10 W/m²K). T_∞, the ambient air temperature (K), was assumed to be equal to the average value of the measured air temperatures along the vertical pole (24.5°C = 297.65 K). σ is the Stefan-Boltzmann constant (W/m²K⁴), ε_{ic} the emissivity of the interior surface of the ceiling (i.e. 1.0 in the experiment), $T_{surf(j)}$ the temperature of each of the other surfaces (K) and $F_{ic \to j}$ the view factor of the ceiling to other surfaces, including the floor and the walls. The view factors of the ceiling to the other surfaces were calculated based on equations presented in Ref. [63] for perpendicular rectangles with a common edge (Table 2). Since different values were measured for surface temperature at 5 different heights of the walls, the view factors of the ceiling to the walls were calculated for 6 portions of walls for which different temperatures were measured in the experiment. Therefore, in Eq. (5), j was 25 including the floor and 6 portions for each wall. $T_{surf(j)}$ for each portion of walls were calculated as the average of the temperatures of the bottom and top line of that portion. The conduction thermal resistance (L/k) of the ceiling was calculated using Eq. (6):

$$\frac{1}{U} = \frac{1}{h_e} + \frac{L}{k} + \frac{1}{h_i} \tag{6}$$

where U is the overall heat transmittance (W/m²K), L the ceiling thickness (m), k the thermal conductivity of the ceiling material (W/mK) and h_e and h_i the exterior and interior surface heat transfer coefficient, respectively. Note that h_e and h_i were assumed to be 10 W/m²K as the combined radiation and convection coefficients based on ISO 6946 [64].

By calculating the thermal resistance (L/k) of the ceiling based on Eq. (6) and knowing other parameters in Eq. (5), the interior surface temperature of the ceiling was calculated to be 24.2°C (297.35 K).

3.3. Solver settings

The commercial CFD code ANSYS/Fluent 12.1 was used to perform the simulations [62]. The 3D steady RANS equations were solved in combination with the Shear-Stress Transport (SST) k-ω model [65]. The SIMPLE algorithm was used for pressure-velocity coupling. Second order discretization schemes were used for both the convection terms and the viscous terms of the governing equations. The PRESTO! scheme was applied for the pressure terms. Because of the temperature-dependent density of the air, the energy and momentum equations were solved simultaneously. Converged solution was assumed to be achieved when the net heat flux imbalance was less than 1% of the smallest heat flux through the domain boundaries. In addition, the velocity magnitudes were monitored at 2 points in the test room until fully converged values were obtained [66]. In the remainder of the paper, the "heat flux criterion (ref. case)" is referred to the criterion used for the reference case.

3.4. Results and comparison with experiment

The CFD results for the reference case, which was outlined in the previous sub-sections, are compared with the full-scale measurements by Li et al. [60]. The difference between the air temperature within the room (T) and the inlet air temperature (T_i) is given as the temperature scale. Figure 5a compares the experimental and CFD results along the vertical pole. The deviations between the measurements and CFD are also depicted in Figure 5b. The general agreement is quite good. CFD underestimates the temperature near the floor and the ceiling and slightly

overestimates it along the other parts of the pole. The main reason for these deviations is not clear. However, it can be related to the assumptions made for the uniform inlet velocity profile and for calculating the surface temperatures of the ceiling and the floor. The average deviation and maximum deviation of the absolute values of the temperature scale between CFD and measurements are 4.2% and 11.9%, respectively.

Figures 6a and b show the air temperature distribution across two vertical planes located 2.1 m from wall 2 and 2.7 m from wall 1, respectively. The first plane intersects the inlet opening and the heat source volume. The second plane intersects the heat source volume and the outlet opening. The distribution of the age of air across the same planes is presented in Figures 6c and d. Figures 6e and f display the velocity vector field across the same planes. As shown in these figures, a plume-type flow caused by the buoyancy effect can be clearly seen above the heat source. This results in the development of recirculation zones and vertical temperature distribution outside the plume. The local age of air is also affected by the vertical temperature stratification outside the plume. The temperature stratification leads to a vertical difference in the air density and therefore an air flow occurs from the lower parts to the upper parts of the room. This air flow impinges on the ceiling and is trapped in the recirculation zones which lead to an increase in the local age of air in the upper regions. The fresh air, entering from the inlet opening, is deflected downward. As a result, the fresh air that has a young age compared to the room air cannot propagate deeply in the room.

4. CFD simulation: sensitivity analysis

A systematic and detailed sensitivity analysis was performed based on the reference case that was outlined in the previous section. To analyze the sensitivity of the results, a single parameter was varied while all other parameters were kept identical to those in the reference case. Then, the results were compared to the reference case to evaluate the impact of the change made on the simulation results. The parameters tested are the resolution of the computational grid (Section 4.1), the turbulence model (Section 4.2), the discretization scheme (Section 4.3) and the convergence criterion (Section 4.4).

4.1. Impact of computational grid resolution

To perform a grid-sensitivity analysis, two additional grids were made: a finer grid and a coarser grid. Refining and coarsening were performed with an overall linear factor $\sqrt{2}$. The coarser grid had 155,382 cells and the finer grid had 1,268,736 cells. The three grids are shown in Figure 7.

The profiles of the temperature scale and the age of air along the pole and two other vertical lines, as shown in Figure 1, for the three grids are presented in Figure 8. The average deviations between the CFD results and measurements for the absolute values of the temperature scale along the pole are 4.2%, 4.2% and 4.0% for the coarse, reference and fine grid, respectively. In this case, the average deviation between the coarse and reference grid along the three lines is 1.7% while it is about 0.9% between the fine and reference grid. For the age of air, these deviations are about 2.7% and 1.6%, respectively. The room average age of air for the coarse, reference and fine grid is about 31.5, 31.3 and 31.0 min, respectively; which shows an absolute deviation of about 0.8% for both the coarse and fine grid from the reference grid. The Grid-Convergence Index (GCI) by Roache [67-68] was used for uniform reporting of this grid convergence study (Figure 9). The results show that the deviation is more noticeable for the lower parts of the pole, line-1 and line-2. For the other parts of these lines, the deviation is negligible. Therefore, the reference grid was retained for further analysis.

4.2. Impact of turbulence model

3D steady RANS CFD simulations were performed with different turbulence models including:
- Standard k-ε model (Sk-ε) [69],
- Realizable k-ε model (Rk-ε) [70],
- Renormalization Group k-ε model (RNG k-ε) [71],
- Standard k-ω model (Sk-ω) [72], and
- Shear-stress transport (SST) k-ω model (SST k-ω) [65].

Note that the Sk-ε, Rk-ε and RNG k-ε model were used in combination with the low-Re number Wolfshtein model [73]. The impact of the choice of turbulence model on the results of the temperature scale and the age of air along the vertical pole, line-1 and line-2 is illustrated in Figure 10.

The average deviations of the absolute values of the temperature scale between CFD and measurements along the pole for Sk-ε, Rk-ε, RNG k-ε, Sk-ω and SST k-ω are 7.0%, 7.9%, 5.6%, 4.9% and 4.2%, respectively. In this case, the maximum deviations of the absolute values are 19.6%, 15.5%, 13.0%, 10.6% and 11.9%, respectively. It can be seen that the SST k-ω model shows the best performance, followed by the Sk-ω model, which also shows a fairly good performance. The differences by the models are pronounced along the pole except near the ceiling. All models tend to overestimate the temperature in the middle of the pole and underestimate it near the ceiling. Note that in several previous studies, the superior performance of the SST k-w model for displacement ventilation has also been pointed

out [22, 54, 56-59]. The success of the prediction could depend on the way in which the boundary layer is modelled. In this study, in order to model the boundary layer accurately, wall functions were not applied but so-called near-wall modelling. All tested turbulence models except the Sk-w and SST k-w models are so-called high-Reynolds number models, which near the wall are replaced by the one-equation Wolfshtein model [73], while the Sk-w and SST k-w models are low-Reynolds number models and are applied all the way down to the wall. However, since the Sk-w model does not show superior performance compared to the high-Re number models, it appears that the near-wall treatment cannot be held responsible for the superior performance of the SST k-w model and the inferior performance of the other four models. As a result, it can be concluded that the SST k-w model predicts the buoyancy-turbulence interaction.

Figures 10d-f clearly show different results for the age of air obtained by different turbulence models along the three lines. The Sk-ω model provides very close results to the SST k-ω model (reference case) with the average deviation of 3.5% along the three lines. The other turbulence models, however, show higher deviations compared to the reference case. In this case, the average deviations of the absolute values along the three lines are 9.0%, 5.7%, and 8.1% for Sk-ε, Rk-ε and RNG k-ε, respectively. In addition, the value for the room average age of air for Sk-ω is almost the same as that for the reference case (i.e. 31.3 min) while it is about 31.5, 30.9 and 30.4 min for Sk-ε, Rk-ε and RNG k-ε, respectively.

Figure 11 shows the velocity vector field across two vertical planes located 2.1 m from wall 2 and 2.7 m from wall 1, respectively, as obtained by the different turbulence models. The plume-type flow and recirculation zones outside the plume are clearly reproduced by the SST k-ω model and the Sk-ω model, but not by the other models. This difference in performance is the reason why the latter models show larger discrepancies along the pole in Figure 10. They poorly reproduce the air flow pattern in the test room.

4.3. Impact of order of discretization scheme

The impact of the order of the discretization scheme on the temperature scale and age of air along the three lines is shown in Figure 12. For the current grid resolution, the impact is rather small: the average deviations of the absolute values of the temperature scale between CFD and measurements along the pole are 5.0% and 4.2% for first-order and second-order discretization schemes, respectively. The deviation between the two schemes for line-2 is less than for the pole and line-1.

For the age of air, the average deviations between the two schemes along the pole, line-1 and line-2 are also small: about 3.1%, 2.2% and 1.6%, respectively. The room average age of air for the first-order discretization scheme is about 31.1 min, which is 0.6% lower than the one with the second-order discretization scheme (reference case).

The small impact of the order of the discretization scheme is attributed to the relatively high grid resolution, which reduces the error by numerical diffusion by the first-order discretization scheme. Even for the first-order calculation on the coarse grid, the results show that the average absolute deviation of the temperature scale between CFD and measurements along the pole is only 4.9%. For the age of air, the average deviations from the reference case, along the pole, line-1 and line-2 are about 5.6%, 3.3% and 3.2%, respectively. And, the room average age of air for the first-order discretization scheme on the coarse grid is about 31.5 min, which is only 0.6% higher than the reference case (Figure 13). It can be concluded that even on a relatively coarse grid (155,382 cells), the impact of the order of the discretization schemes is minor.

4.4. Impact of level of iterative convergence

In literature, there is no general agreement on the required level of iterative convergence for an adequately-converged solution. Too lenient convergence criteria should be avoided. For instance, the default setting of scaled residuals in Fluent 6.3 is 10^{-3}, which is a rather high and lenient value [29], although the ANSYS training manual has presented tighter criteria to check whether a converged solution has been achieved [66]. In some previous studies, much more stringent convergence criteria were imposed [14, 28, 74-76]. In this section, the impact of three different minimum thresholds of scaled residuals on the results is investigated. For these three cases, a converged solution was assumed to be obtained when all the scaled residuals levelled off and reached a minimum of the prescribed value (i.e. 10^{-3}, 10^{-4} and 10^{-8}).

Figure 14 shows the profiles of the temperature scale and age of air along the lines for the three thresholds. It can be seen that the level of iterative convergence has a significant impact on the results of the age of air. This is especially the case for the thresholds of 10^{-3} and 10^{-4}, where the average deviations from the reference case are 14.9% and 12.9%, respectively. For the temperature scale, however, these deviations are less, i.e. 1.4% and 0.4%. Figure 14 also confirms that the 10^{-8} threshold results in almost the same results as those of the reference case for both the temperature scale and the age of air. Note that further reduction in the minimum threshold of scaled residuals has no significant impact on the results (not shown in this figure).

Figure 15 shows the distribution of the age of air in the vertical planes for the reference case and for the 10^{-3}, 10^{-4} and 10^{-8} thresholds. It shows that 10^{-3} and 10^{-4} thresholds result in substantial deviations from the reference case. However, the 10^{-8} threshold yields the same distribution of the age of air as the reference case. The room average age

of air for the 10^{-3} and 10^{-4} threshold are about 26.8 and 27.8 min, which shows a deviation of 14.3% and 11.2% from the reference case. The 10^{-8} threshold provides the same value for the room average age of air (i.e. 31.3 min).

5. Discussion

It is important to mention some limitations of this study:

- In this study, a room with a heat source and two ventilation openings was considered. Earlier studies have shown the importance of different physical parameters on the performance of displacement ventilation systems, such as supply air velocity and temperature [10, 43], room geometry [16, 46, 77], intensity [10, 16], location [78], size [79-80] and number of heat sources [81-82], size [16, 77, 81], number [43, 77, 81] and location of openings [44] and air change rate [43, 79]. Further research is therefore needed to evaluate the performance of steady RANS CFD simulations to predict the performance of this type of ventilation under different physical characteristics.
- This study was performed for a single isolated building space and the influence of connected interior spaces was not included. Further research is needed on the validation, verification and sensitivity analysis of steady RANS CFD simulations for the stratified indoor environment in more complex spaces.
- The study only considered steady RANS CFD simulations, as the purpose was to investigate how well steady RANS CFD would be able to predict the temperature stratification within a room with a heat source and two ventilation openings. In spite of the well-known deficiencies of steady RANS, a good agreement was obtained between CFD simulations and measurements. Obtaining a better agreement here would necessitate the use of Large Eddy Simulation (LES), which however is much more computationally expensive than steady RANS.
- Further research is necessary on exploring the impact of radiative heat transfer between the interior surfaces and conductive heat transfer through the walls.

6. Conclusions

Knowledge of temperature stratification in indoor environments is required for occupants' local thermal comfort. In addition, in higher building spaces, such as atriums, temperature stratification is important for providing thermal comfort in the lower and upper adjacent spaces. This phenomenon also affects the indoor air quality by causing a vertical difference in local age of air.

In this paper, a detailed and systematic assessment of 3D steady RANS CFD simulations was performed for determining the air temperature distribution and for evaluating the air quality caused by temperature stratification within a space with a heat source and two ventilation openings. This paper is intended to contribute to improved accuracy and reliability of CFD simulations for displacement ventilation assessment.

The following conclusions are obtained:

- Although the amount of experimental data is limited, the validation study shows that the 3D steady RANS approach with the SST k-ω can accurately predict the vertical temperature profile and stratification.
- The use of three different computational grids (155,382 cells, 451,248 cells and 1,268,736 cells) indicates that the grid resolution only has a minor influence on the resulting vertical profiles of temperature and age of air.
- The impact the turbulence model however is very large. Out of the five commonly used turbulence models tested, the Sk-ε, Rk-ε, RNG k-ε, Sk-ω and SST k-ω model, only the two k-ω models succeed in reproducing the thermal plume structure and the associated thermal stratification, while the three k-ε models clearly fail in doing so.
- The impact of the order of the discretization schemes is minor, even for the coarsest grid (155,382), which indicates that numerical diffusion is limited and/or does not substantially affect the results in terms of temperature and age of air.
- Finally, the iterative convergence criteria have a very large impact on the results of the age of air, where it is shown that very stringent criteria in terms of scaled residuals are required to obtain accurate results. These required criteria are much more stringent than typical default settings.

Nomenclature

σ = Stefan-Boltzmann constant (W/m^{2}K^4)
ε_i = surface emissivity (-)
q''_{cond} = conduction heat flux (W/m^2)
q''_{conv} = convection heat flux (W/m^2)
q''_{rad} = radiation heat flux (W/m^2)
$\bar{u}$ = inlet air velocity (m/s)
A_f = floor surface area (m^2)
A_i = inlet opening area (m^2)

c_p = specific heat capacity of air (J/kgK)
E = heat load (W)
h_{ci} = interior convective heat transfer coefficient (W/m^{2}K)
h_e = exterior surface heat transfer coefficient (W/m^{2}K)
h_i = interior surface heat transfer coefficient (W/m^{2}K)
k = thermal conductivity (W/mK)
L = thickness (m)
n = number of test-room air changes (1/s)
Pr = molecular Prandtl number (-)
Q = inlet flow rate (m^3/s)
q = volumetric heat generation (W/m^3)
Ra = Rayleigh number (-)
T_f^a = near-floor air temperature (°C)
T_∞ = ambient air temperature (K)
T_{ec} = exterior surface temperature of the ceiling (K)
T_i = inlet air temperature (°C)
T_{ic} = interior surface temperature of the ceiling (K)
T_{if} = floor surface temperature (°C)
T_o = outlet air temperature (°C)
T_{surf} = surface temperature (K)
U = overall heat transmittance (W/m^{2}K)
V = test-room volume (m^3)
V_{hs} = heat-source volume (m^3)
ρ = air density (kg/m^3)

References

[1] Sandberg M, Sjöberg M. The use of moments for assessing air quality in ventilated rooms. Building and Environment. 1983;18:181-97.
[2] Etheridge D. Natural ventilation of buildings: Theory, measurement and design: John Wiley & Sons, Ltd.; 2012.
[3] Buratti C, Mariani R, Moretti E. Mean age of air in a naturally ventilated office: Experimental data and simulations. Energy and Buildings. 2011;43:2021-7.
[4] Meiss A, Feijó-Muñoz J, García-Fuentes MA. Age-of-the-air in rooms according to the environmental condition of temperature: A case study. Energy and Buildings. 2013;67:88-96.
[5] Wang Y, Zhao F-Y, Kuckelkorn J, Liu D, Liu J, Zhang J-L. Classroom energy efficiency and air environment with displacement natural ventilation in a passive public school building. Energy and Buildings. 2014;70:258-70.
[6] Hussain S, Oosthuizen PH. Numerical investigations of buoyancy-driven natural ventilation in a simple three-storey atrium building and thermal comfort evaluation. Applied Thermal Engineering. 2013;57:133-46.
[7] Hussain S, Oosthuizen PH. Numerical investigations of buoyancy-driven natural ventilation in a simple atrium building and its effect on the thermal comfort conditions. Applied Thermal Engineering. 2012;40:358-72.
[8] Lin Z, Chow TT, Tsang CF. Effect of door opening on the performance of displacement ventilation in a typical office building. Building and Environment. 2007;42:1335-47.
[9] Saïd MNA, MacDonald RA, Durrant GC. Measurement of thermal stratification in large single-cell buildings. Energy and Buildings. 1996;24:105-15.
[10] Xu M, Yamanaka T, Kotani H. Vertical profiles of temperature and contaminant concentration in rooms ventilated by displacement with heat loss through room envelopes. Indoor Air. 2001;11:111-9.
[11] Wan MP, Chao CY. Numerical and experimental study of velocity and temperature characteristics in a ventilated enclosure with underfloor ventilation systems. Indoor Air. 2005;15:342-55.
[12] Crouzeix C, Le Mouël JL, Perrier F, Richon P. Thermal stratification induced by heating in a non-adiabatic context. Building and Environment. 2006;41:926-39.
[13] Awad AS, Calay RK, Badran OO, Holdo AE. An experimental study of stratified flow in enclosures. Applied Thermal Engineering. 2008;28:2150-8.
[14] van Hooff T, Blocken B. Coupled urban wind flow and indoor natural ventilation modelling on a high-resolution grid: A case study for the Amsterdam ArenA stadium. Environmental Modelling and Software. 2010;25:51-65.
[15] van Hooff T, Blocken B. CFD evaluation of natural ventilation of indoor environments by the concentration decay method: CO2 gas dispersion from a semi-enclosed stadium. Building and Environment. 2013;61:1-17.
[16] Cooper P, Linden PF. Natural ventilation of an enclosure containing two buoyancy sources. Journal of Fluid Mechanics. 1996;311:153-76.
[17] Tovar R, Linden PF, Thomas LP. Hybrid ventilation in two interconnected rooms with a buoyancy source. Solar Energy. 2007;81:683-91.

[18] Nielsen PV, Restivo A, Whitelaw JH. Buoyancy-affected flows in ventilated rooms. Numerical Heat Transfer, Part A. 1979;2:115-27.

[19] Li Y, Sandberg M, Fuchs L. Vertical temperature profiles in rooms ventilated by displacement: Full-scale measurement and nodal modelling. Indoor Air. 1992;2:225-43.

[20] Li Y. Buoyancy-driven natural ventilation in a thermally stratified one-zone building. Building and Environment. 2000;35:207-14.

[21] Crouzeix C, Le Mouël JL, Perrier F, Richon P. Non-adiabatic boundaries and thermal stratification in a confined volume. International Journal of Heat and Mass Transfer. 2006;49:1974-80.

[22] Stamou A, Katsiris I. Verification of a CFD model for indoor airflow and heat transfer. Building and Environment. 2006;41:1171-81.

[23] Chen Q. Ventilation performance prediction for buildings: A method overview and recent applications. Building and Environment. 2009;44:848-58.

[24] Hensen JLM, Hamelinck MJH. Energy simulation of displacement ventilation in offices. Building Services Engineering Research and Technology. 1995;16:77-81.

[25] Blocken B. 50 years of Computational Wind Engineering: Past, present and future. Journal of Wind Engineering and Industrial Aerodynamics. 2014;129:69-102.

[26] Tominaga Y, Mochida A, Yoshie R, Kataoka H, Nozu T, Yoshikawa M, et al. AIJ guidelines for practical applications of CFD to pedestrian wind environment around buildings. Journal of Wind Engineering and Industrial Aerodynamics. 2008;96:1749-61.

[27] Blocken B, Stathopoulos T, Carmeliet J, Hensen JLM. Application of computational fluid dynamics in building performance simulation for the outdoor environment: An overview. Journal of Building Performance Simulation. 2011;4:157-84.

[28] Montazeri H, Blocken B. CFD simulation of wind-induced pressure coefficients on buildings with and without balconies: Validation and sensitivity analysis. Building and Environment. 2013;60:137-49.

[29] Blocken B. Computational Fluid Dynamics for urban physics: Importance, scales, possibilities, limitations and ten tips and tricks towards accurate and reliable simulations. Building and Environment. 2015: In Press.

[30] Yang C, Demokritou P, Chen Q, Spengler J. Experimental validation of a computational fluid qynamics model for IAQ applications in Ice Rink Arenas. Indoor Air. 2001;11:120-6.

[31] Hayashi T, Ishizu Y, Kato S, Murakami S. CFD analysis on characteristics of contaminated indoor air ventilation and its application in the evaluation of the effects of contaminant inhalation by a human occupant. Building and Environment. 2002;37:219-30.

[32] Sørensen DN, Nielsen PV. Quality control of computational fluid dynamics in indoor environments. Indoor Air. 2003;13:2-17.

[33] Nielsen PV. Computational fluid dynamics and room air movement. Indoor Air. 2004;14:134-43.

[34] van Hooff T, Blocken B, van Heijst GJF. On the suitability of steady RANS CFD for forced mixing ventilation at transitional slot Reynolds numbers. Indoor Air. 2013;23:236-49.

[35] Gao CF, Lee WL. Evaluating the influence of openings configuration on natural ventilation performance of residential units in Hong Kong. Building and Environment. 2011;46:961-9.

[36] Bangalee MZI, Lin SY, Miau JJ. Wind driven natural ventilation through multiple windows of a building: A computational approach. Energy and Buildings. 2012;45:317-25.

[37] Ramponi R, Blocken B. CFD simulation of cross-ventilation for a generic isolated building: Impact of computational parameters. Building and Environment. 2012;53:34-48.

[38] Montazeri H. Experimental and numerical study on natural ventilation performance of various multi-opening wind catchers. Building and Environment. 2011;46:370-8.

[39] Montazeri H, Montazeri F, Azizian R, Mostafavi S. Two-sided wind catcher performance evaluation using experimental, numerical and analytical modeling. Renewable Energy. 2010;35:1424-35.

[40] Montazeri H, Azizian R. Experimental study on natural ventilation performance of a two-sided wind catcher. Proceedings of the Institution of Mechanical Engineers, Part A: Journal of Power and Energy. 2009;223:387-400.

[41] Howell SA, Potts I. On the natural displacement flow through a full-scale enclosure, and the importance of the radiative participation of the water vapour content of the ambient air. Building and Environment. 2002;37:817-23.

[42] Cook MJ, Lomas KJ. Buoyancy-driven displacement ventilation flows: Evaluation of two eddy viscosity turbulence models for prediction. Building Services Engineering Research and Technology. 1998;19:15-21.

[43] Kobayashi N, Chen Q. Floor-Supply Displacement Ventilation in a Small Office. Indoor and Built Environment. 2003;12:281-91.

[44] Lin Z, Chow TT, Tsang CF, Fong KF, Chan LS. CFD study on effect of the air supply location on the performance of the displacement ventilation system. Building and Environment. 2005;40:1051-67.

[45] Ji Y, Cook MJ. Numerical studies of displacement natural ventilation in multi-storey buildings connected to an atrium. Building Services Engineering Research and Technology. 2007;28:207-22.

[46] Ji Y, Cook MJ, Hanby V. CFD modelling of natural displacement ventilation in an enclosure connected to an atrium. Building and Environment. 2007;42:1158-72.

[47] Liu P-C, Lin H-T, Chou J-H. Evaluation of buoyancy-driven ventilation in atrium buildings using computational fluid dynamics and reduced-scale air model. Building and Environment. 2009;44:1970-9.

[48] Cheng Y, Niu J, Gao N. Stratified air distribution systems in a large lecture theatre: A numerical method to optimize thermal comfort and maximize energy saving. Energy and Buildings. 2012;55:515-25.

[49] Jiang Y, Chen Q. Buoyancy-driven single-sided natural ventilation in buildings with large openings. International Journal of Heat and Mass Transfer. 2003;46:973-88.

[50] Gladstone C, Woods AW. On buoyancy-driven natural ventilation of a room with a heated floor. Journal of Fluid Mechanics. 2001;441:293-314.

[51] Gan G. Simulation of buoyancy-driven natural ventilation of buildings—Impact of computational domain. Energy and Buildings. 2010;42:1290-300.

[52] Walker C, Tan G, Glicksman L. Reduced-scale building model and numerical investigations to buoyancy-driven natural ventilation. Energy and Buildings. 2011;43:2404-13.

[53] Xing H, Hatton A, Awbi HB. A study of the air quality in the breathing zone in a room with displacement ventilation. Building and Environment. 2001;36:809-20.

[54] Zhang T, Lee K, Chen Q. A simplified approach to describe complex diffusers in displacement ventilation for CFD simulations. Indoor Air. 2009;19:255-67.

[55] Lin Z, Chow TT, Wang Q, Fong KF, Chan LS. Validation of CFD model for research into displacement ventilation. Architectural Science Review. 2005;48:305-16.

[56] Zhai ZJ, Zhang Z, Zhang W, Chen QY. Evaluation of various turbulence models in predicting airflow and turbulence in enclosed environments by CFD: Part 1—Summary of prevalent turbulence models. HVAC&R Research. 2007;13:853-70.

[57] Zhang Z, Zhang W, Zhai ZJ, Chen QY. Evaluation of various turbulence models in predicting airflow and turbulence in enclosed environments by CFD: Part 2—Comparison with experimental data from literature. HVAC&R Research. 2007;13:871-86.

[58] Hussain S, Oosthuizen PH. Validation of numerical modeling of conditions in an atrium space with a hybrid ventilation system. Building and Environment. 2012;52:152-61.

[59] Hussain S, Oosthuizen PH, Kalendar A. Evaluation of various turbulence models for the prediction of the airflow and temperature distributions in atria. Energy and Buildings. 2012;48:18-28.

[60] Li Y, Sandberg M, Fuchs L. Effects of thermal radiation on airflow with displacement ventilation: An experimental investigation. Energy and Buildings. 1993;19:263-74.

[61] Sandberg M. What is ventilation efficiency? Building and Environment. 1981;16:123-35.

[62] ANSYS. ANSYS Fluent 12.0 user's guide: ANSYS, Inc.; 2009.

[63] Bergman TL, Lavine AS, Incropera FP, Dewitt DP. Fundamentals of heat and mass transfer. Seventh ed: John Wiley and Sons, Inc.; 2011.

[64] ISO. Building components and building elements - Thermal resistance and thermal transmittance - Calculation method (ISO 6946:2007). Second ed: International Organization for Standardization; 2007.

[65] Menter FR. Two-equation eddy-viscosity turbulence models for engineering applications. AIAA Journal. 1994;32:1598-605.

[66] ANSYS. Introductory FLUENT training - Chapter 5: Solver settings: ANSYS, Inc.; 2009.

[67] Roache PJ. Perspective: A method for uniform reporting of grid refinement studies. Journal of Fluids Engineering. 1994;116:405-13.

[68] Roache PJ. Quantification of uncertainty in computational fluid dynamics. Annual Review of Fluid Mechanics. 1997;29:123-60.

[69] Launder BE, Spalding DB. Lectures in mathematical models of turbulence. London, England: Academic Press; 1972.

[70] Shih T-H, Liou WW, Shabbir A, Yang Z, Zhu J. A new k-ϵ eddy viscosity model for high reynolds number turbulent flows. Computers and Fluids. 1995;24:227-38.

[71] Yakhot V, Orszag S. Renormalization group analysis of turbulence. I. Basic theory. Journal of Scientific Computing. 1986;1:3-51.

[72] Wilcox DC. Turbulence modeling for CFD. La Canada, California: DCW Industries, Inc.; 1998.

[73] Wolfshtein M. The velocity and temperature distribution in one-dimensional flow with turbulence augmentation and pressure gradient. International Journal of Heat and Mass Transfer. 1969;12:301-18.

[74] van Hooff T, Blocken B, Aanen L, Bronsema B. A venturi-shaped roof for wind-induced natural ventilation of buildings: Wind tunnel and CFD evaluation of different design configurations. Building and Environment. 2011;46:1797-807.

[75] Blocken B, Janssen WD, van Hooff T. CFD simulation for pedestrian wind comfort and wind safety in urban areas: General decision framework and case study for the Eindhoven University campus. Environmental Modelling & Software. 2012;30:15-34.

[76] Montazeri H, Blocken B, Janssen WD, van Hooff T. CFD evaluation of new second-skin facade concept for wind comfort on building balconies: Case study for the Park Tower in Antwerp. Building and Environment. 2013;68:179-92.

[77] Chen ZD, Li Y. Buoyancy-driven displacement natural ventilation in a single-zone building with three-level openings. Building and Environment. 2002;37:295-303.

[78] Park H-J, Holland D. The effect of location of a convective heat source on displacement ventilation: CFD study. Building and Environment. 2001;36:883-9.

[79] Auban O, Lemoine F, Vallette P, Fontaine JR. Simulation by solutal convection of a thermal plume in a confined stratified environment: application to displacement ventilation. International Journal of Heat and Mass Transfer. 2001;44:4679-91.

[80] Bouzinaoui A, Vallette P, Lemoine F, Fontaine JR, Devienne R. Experimental study of thermal stratification in ventilated confined spaces. International Journal of Heat and Mass Transfer. 2005;48:4121-31.

[81] Linden PF, Lane-Serff GF, Smeed DA. Emptying filling boxes: the fluid mechanics of natural ventilation. Journal of Fluid Mechanics. 1990;212:309-35.

[82] Linden PF, Cooper P. Multiple sources of buoyancy in a naturally ventilated enclosure. Journal of Fluid Mechanics. 1996;311:177-92.
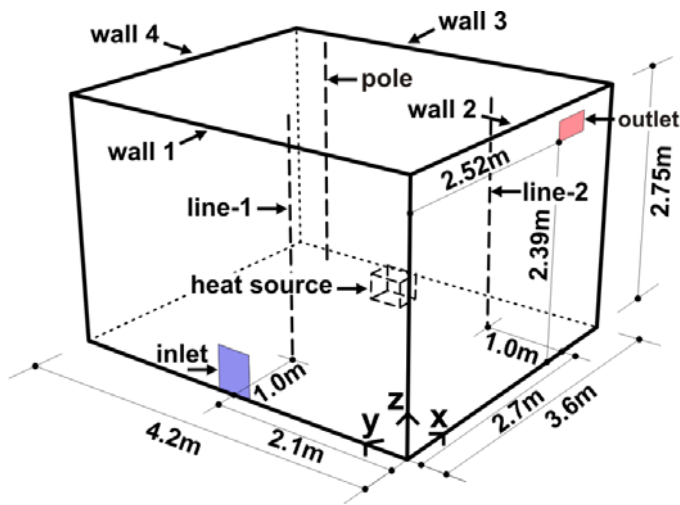
Figure 1. Geometry of the test room: position of the inlet and outlet openings, heat source and vertical pole, line-1 and line-2.
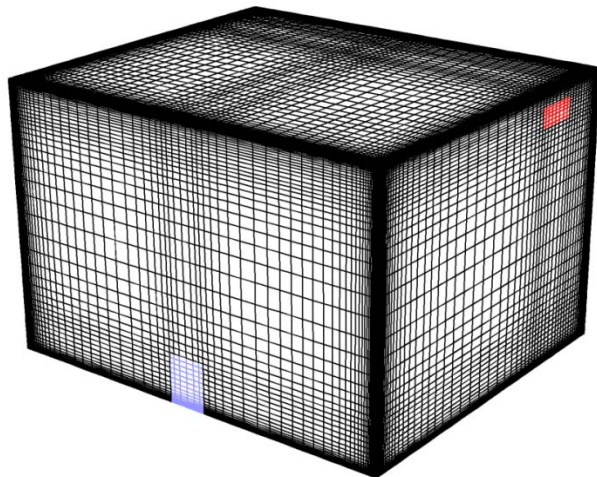
Figure 2. Perspective view of high-resolution computational grid on three walls of the test room (total number of cells: 451,248).
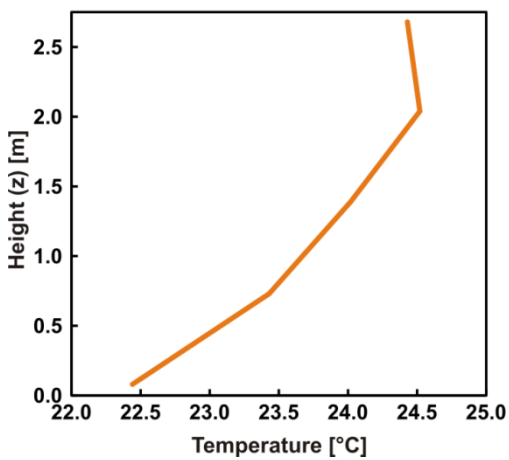
Figure 3. Interior surface temperature of vertical walls at different heights imposed by user-defined functions (UDFs) in the CFD simulations.
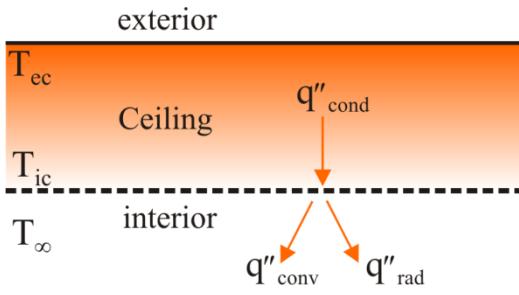
Figure 4. Energy balance at the interior surface of the ceiling.
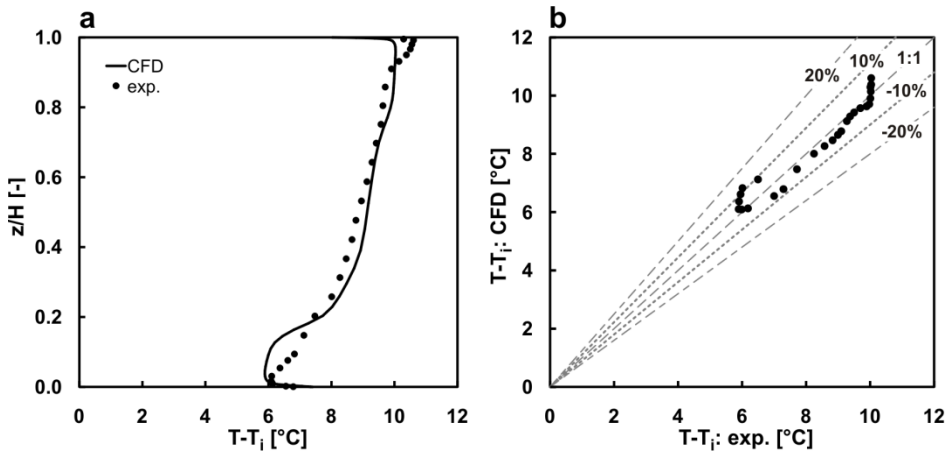
Figure 5. (a, b) Comparison of temperature difference $(T - T_i)$ by CFD simulation and experimental results.
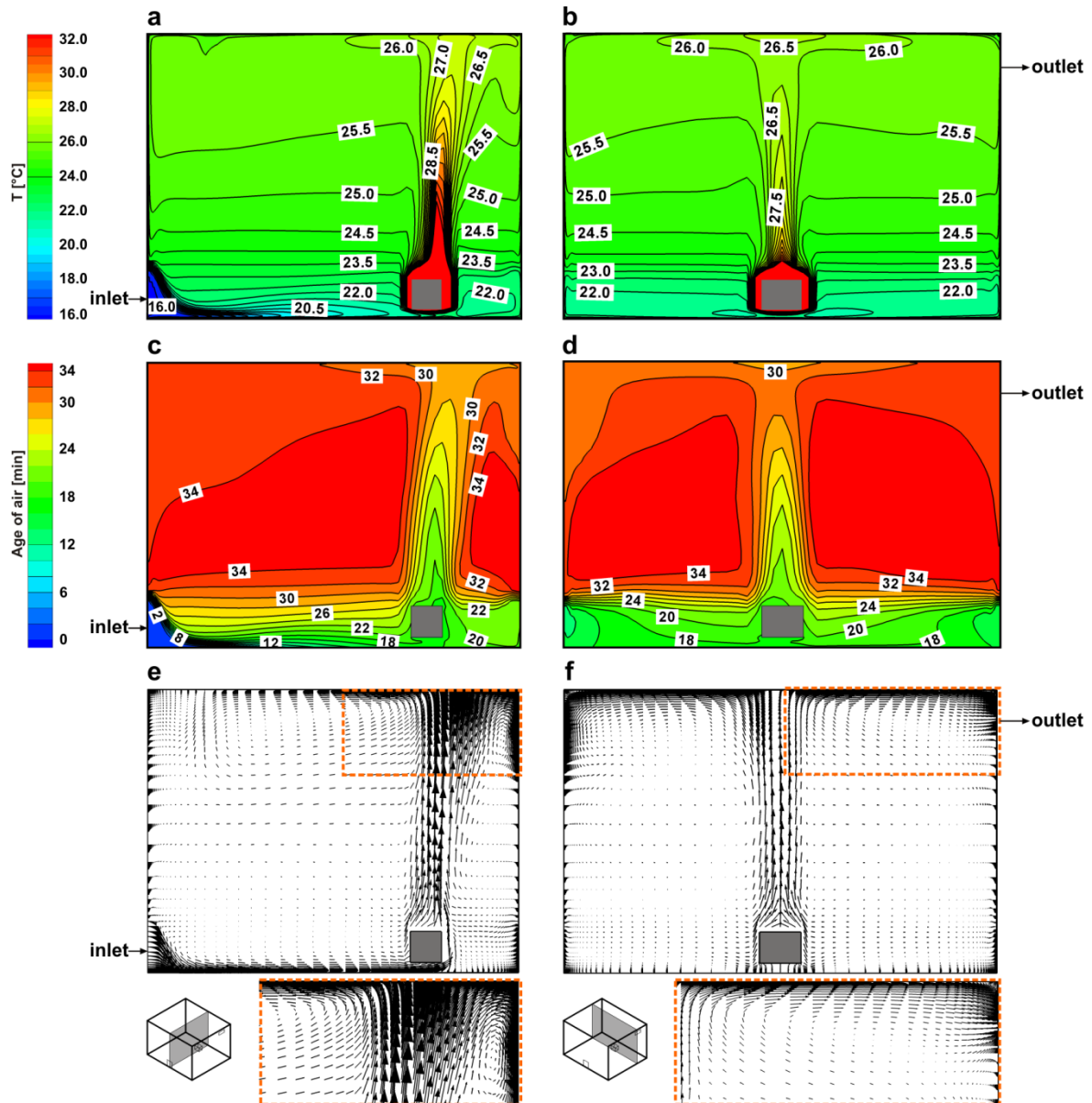
Figure 6. (a, b) Distribution of air temperature, (c, d) age of air and (e, f) velocity vector field across two vertical planes.
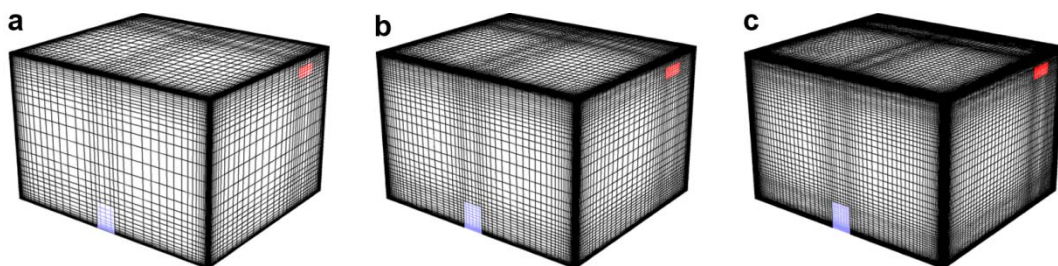
Figure 7. Computational grids for grid-sensitivity analysis: (a) coarse grid (155,382 cells), (b) reference grid (451,248 cells) and (c) fine grid (1,268,736 cells).
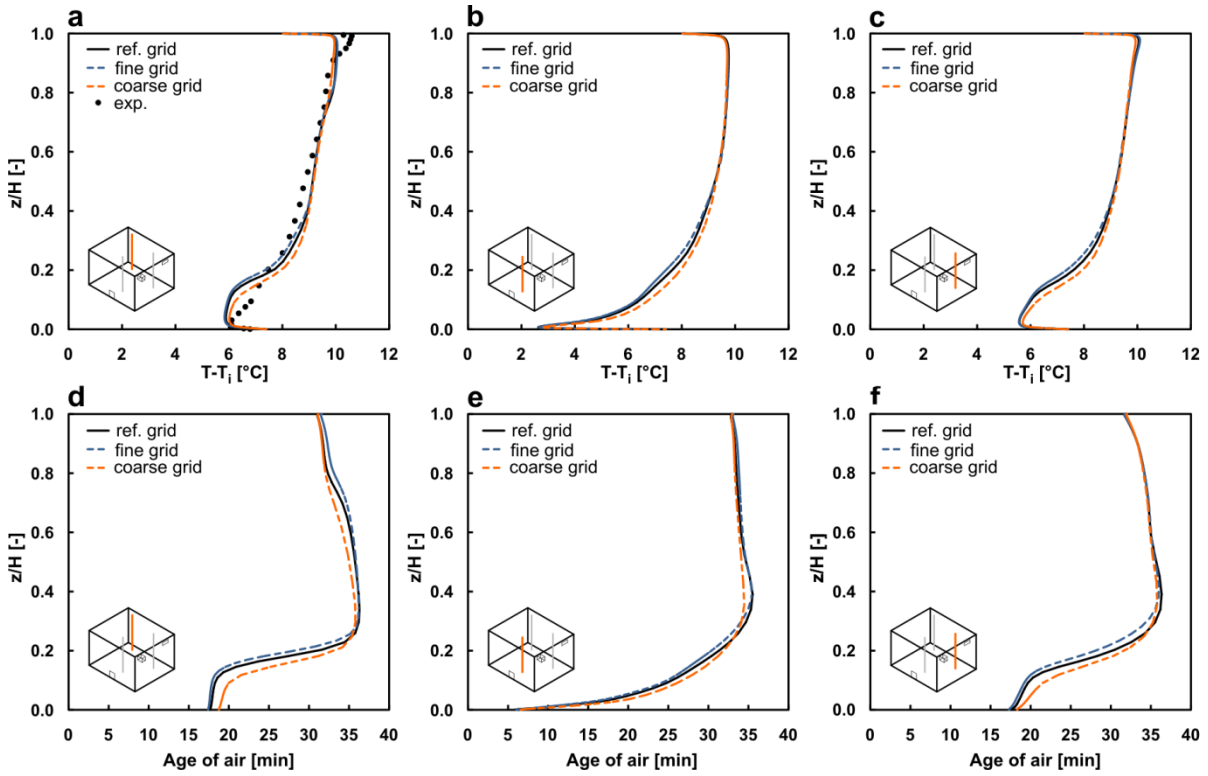
Figure 8. Impact of grid resolution on: (a-c) profile of temperature difference and (d-f) age of air, along three vertical lines.
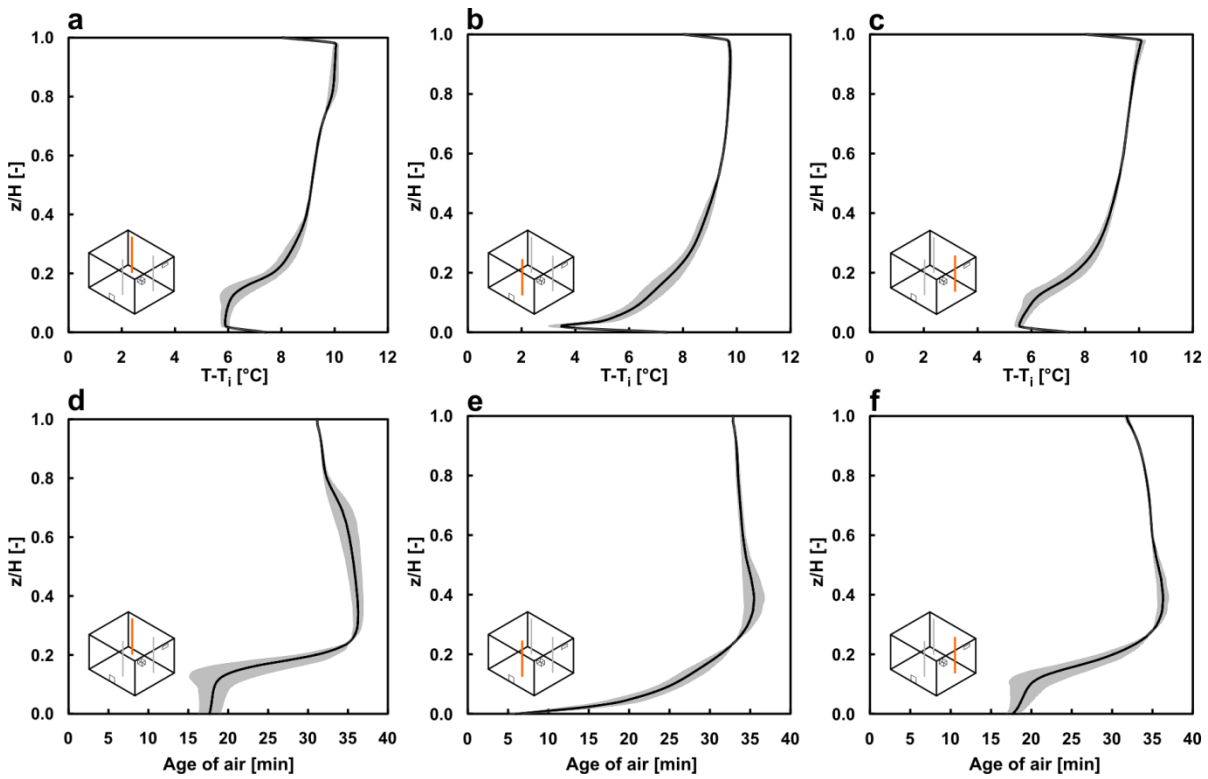
Figure 9. Impact of grid resolution on: (a-c) profile of temperature difference and (d-f) age of air, along three vertical lines, with error band of grid convergence index by Roache [67-68].
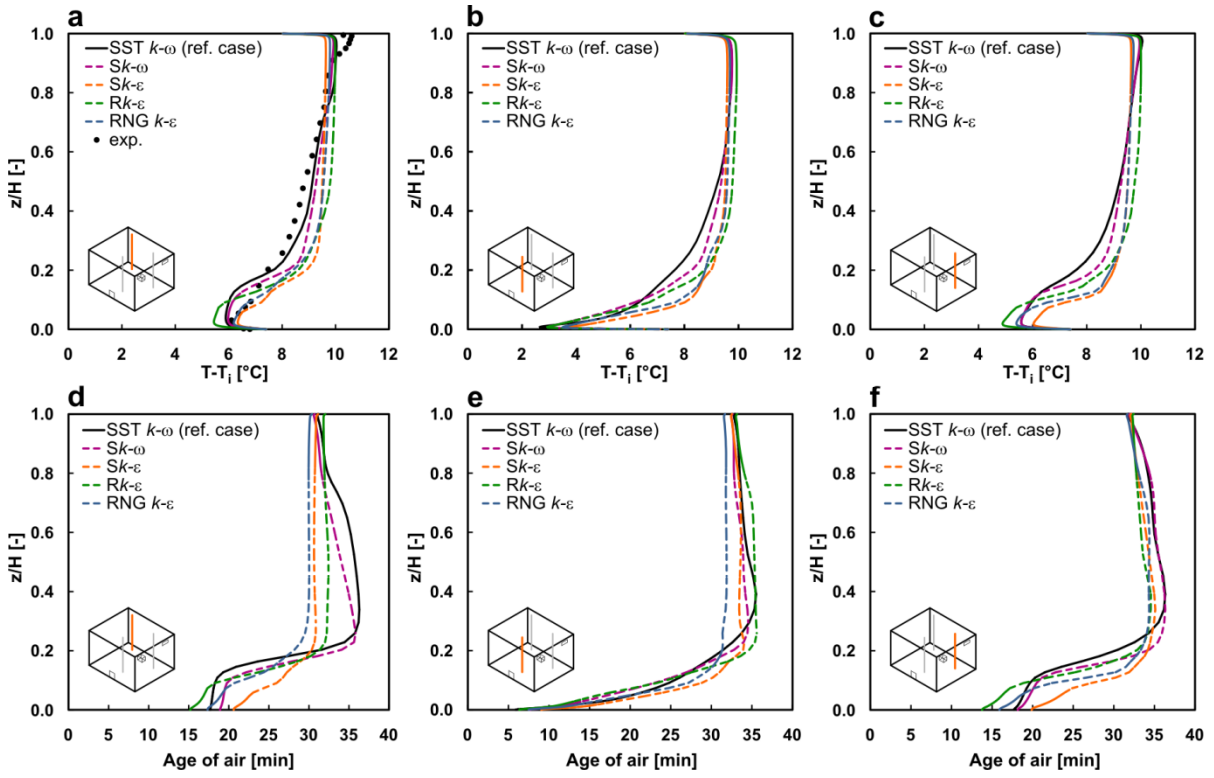
Figure 10. Impact of turbulence model on: (a-c) profiles of temperature scale and (d-f) age of air, along three vertical lines.
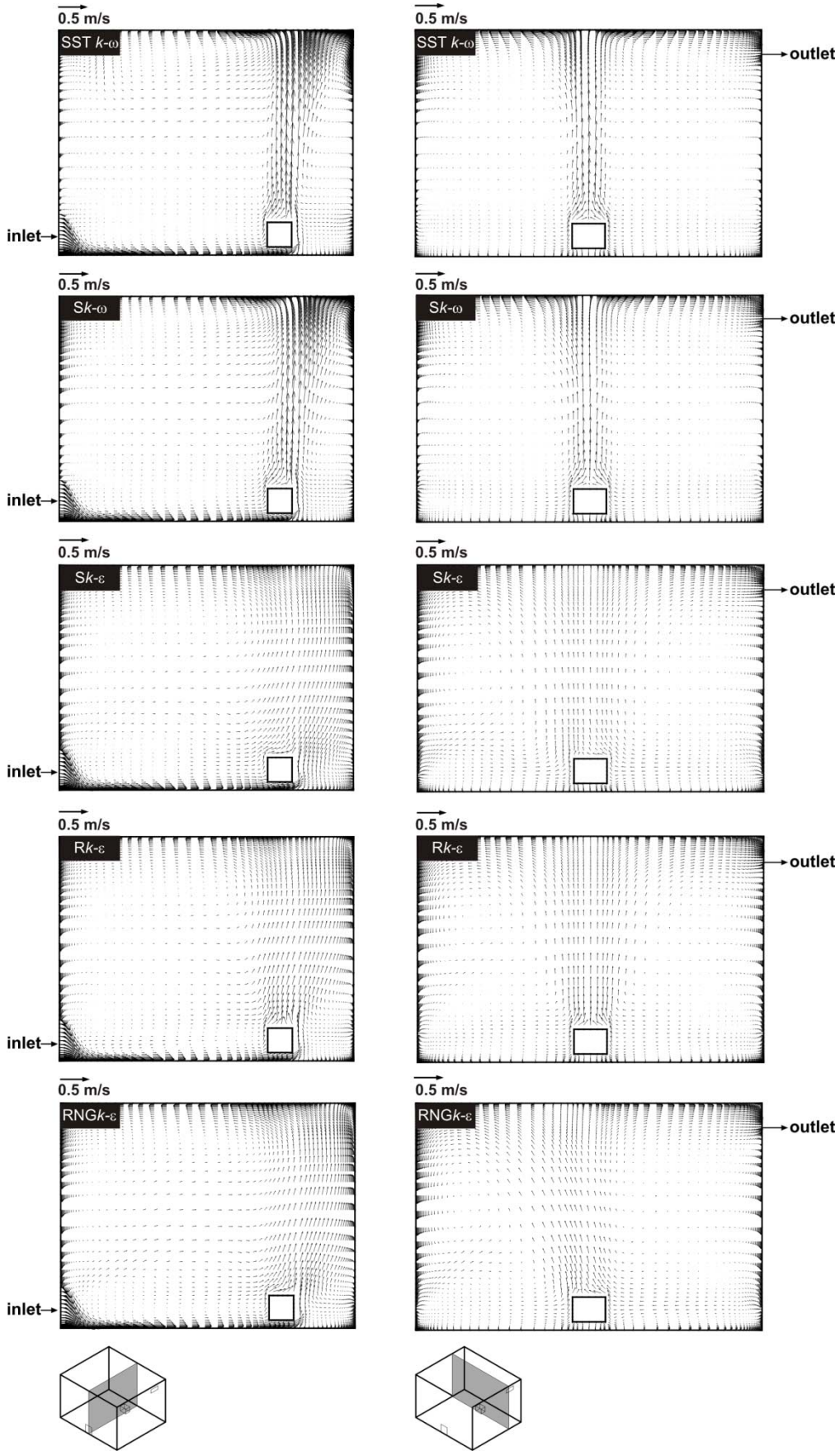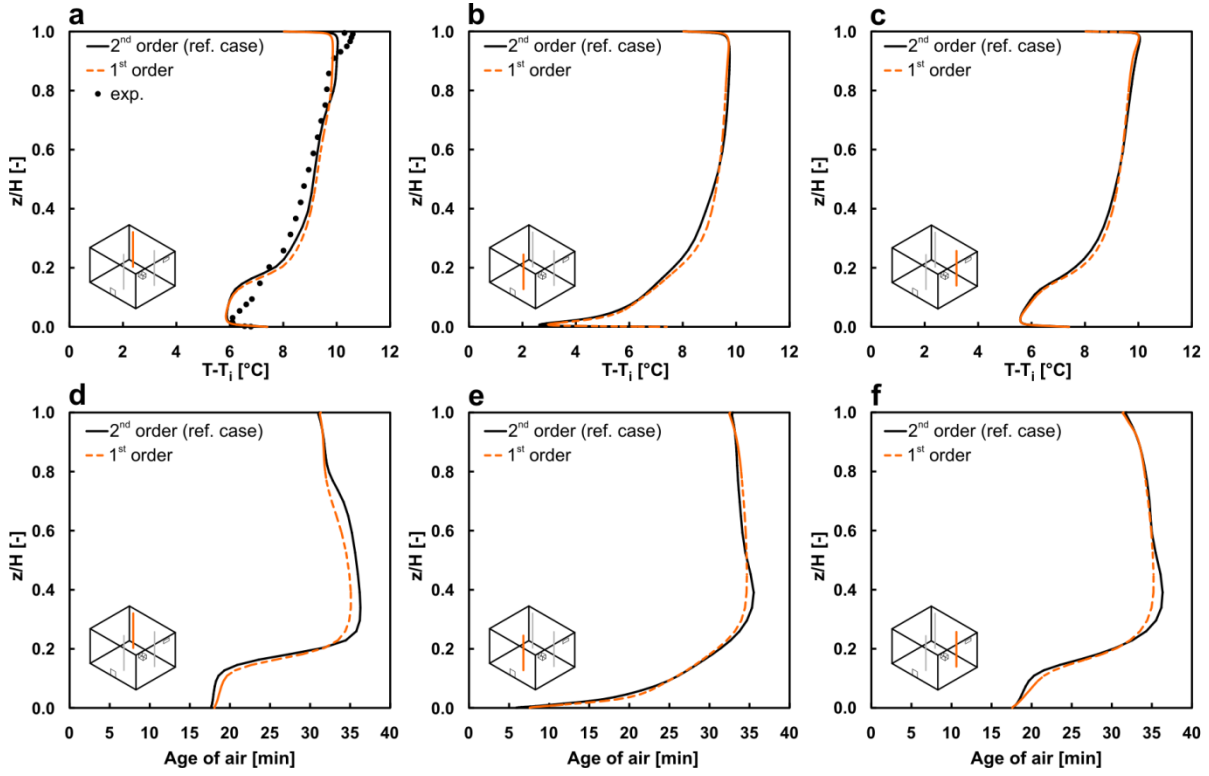
Figure 11. Impact of turbulence model on velocity vector field across two vertical planes: (a, b) SST *k-ω*, (c, d) *Sk-ω*, (e, f) S*k-ε*, (g, h) R*k-ε*, (i, j) RNG *k-ε*.

17

Figure 12. Impact of order of discretization scheme on: (a-c) profiles of temperature difference and (d-f) age of air, along three vertical lines.
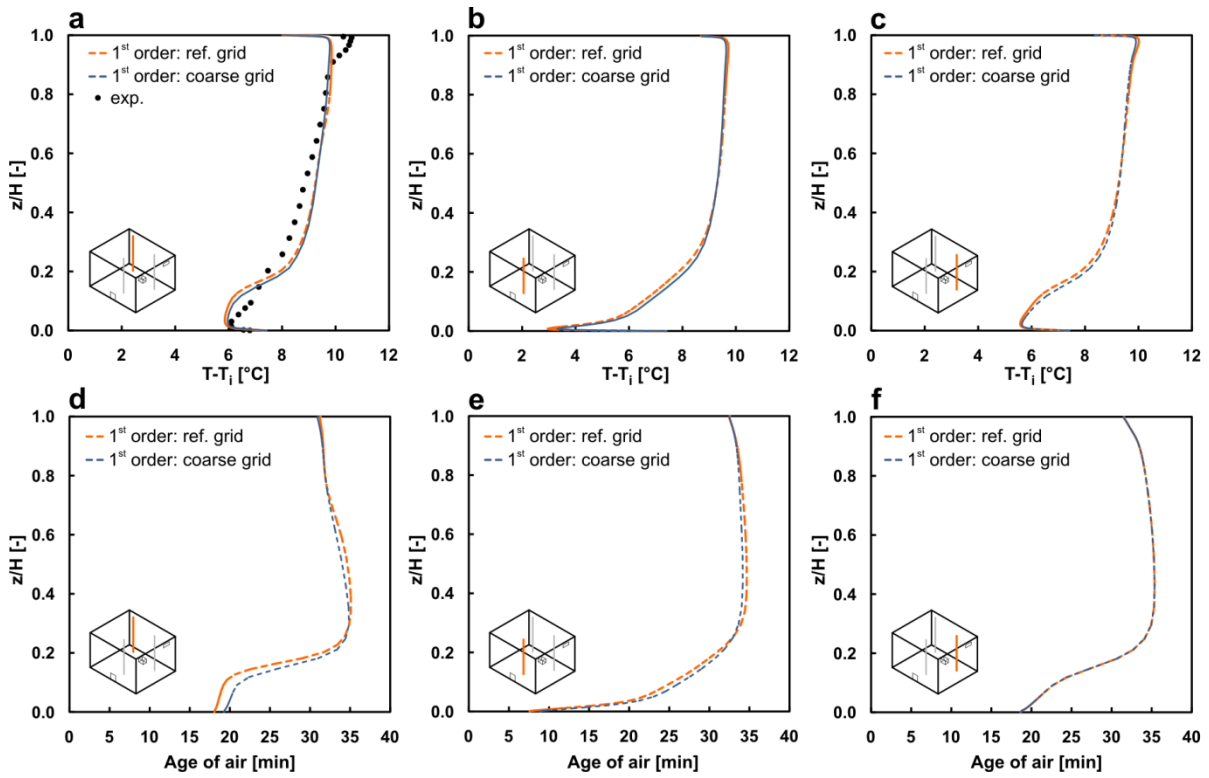

Figure 13. Comparison of the first-order discretization scheme on the reference and coarse grid: (a-c) profiles of temperature difference and (d-f) age of air, along three vertical lines.
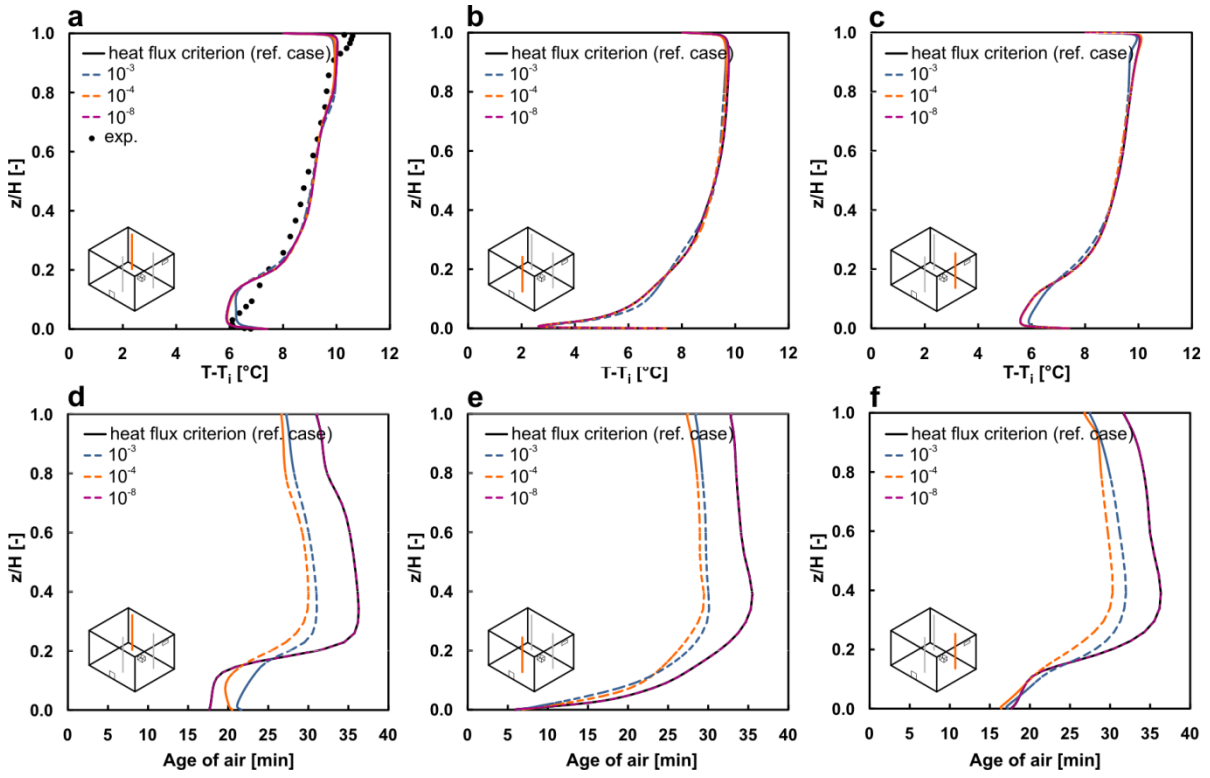
Figure 14. Impact of iterative convergence limit for the reference case and the different thresholds for the scaled residuals 10^{-3}, 10^{-4} and 10^{-8} on: (a-c) profiles of temperature difference and (d-f) age of air, along three vertical lines.
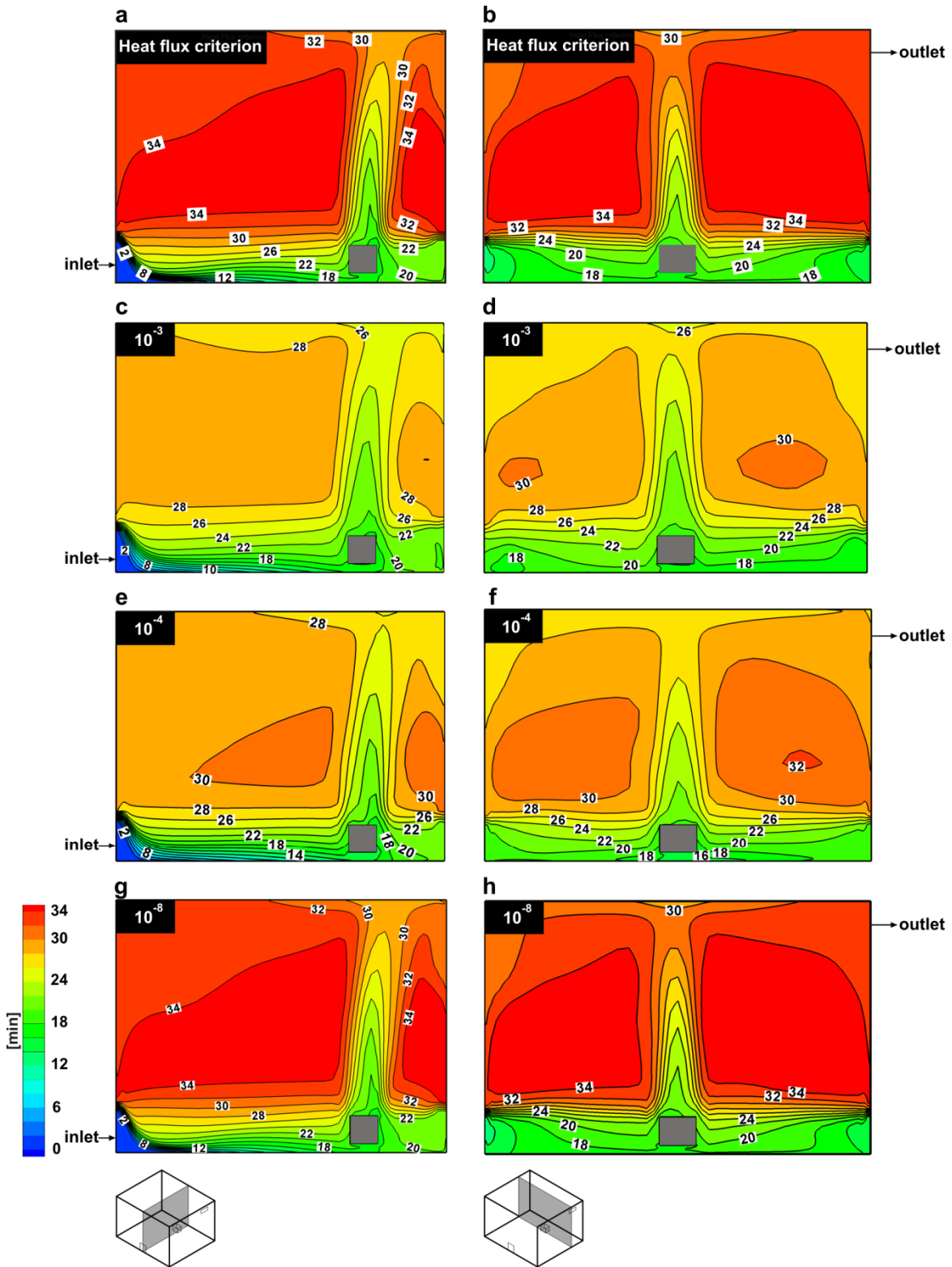
Figure 15. Impact of iterative convergence limit on distribution of age of air across two vertical planes for: (a, b) reference case, (c, d) minimum thresholds for scaled residuals of 10^{-3}, (e, f) 10^{-4} and (g, h) 10^{-8}.